J. Fluid Mech. (2023), *vol*. 977, A24, doi:10.1017/jfm.2023.948

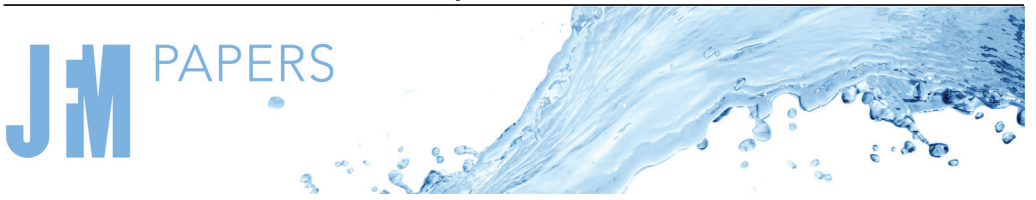

Droplet jumping by modulated electrowetting

Quoc Vo[1],† **and Tuan Tran**[2],†

[1]School of Medicine, University of Pittsburgh, 4200 Fifth Ave, Pittsburgh, PA 15260, USA

[2]School of Mechanical & Aerospace Engineering, Nanyang Technological University, 50 Nanyang Avenue, 639798, Republic of Singapore

(Received 26 April 2023; revised 30 October 2023; accepted 3 November 2023)

We investigate jumping of sessile droplets from a solid surface in ambient oil using modulated electrowetting actuation. We focus on the case in which the electrowetting effect is activated to cause droplet spreading and then deactivated exactly at the moment the droplet reaches its maximum deformation. By systematically varying the control parameters such as the droplet radius, liquid viscosity and applied voltage, we provide detailed characterisation of the resulting behaviours including a comprehensive phase diagram separating detachment from non-detachment behaviours, as well as how the detach velocity and detach time, i.e. duration leading to detachment, depend on the control parameters. We then construct a theoretical model predicting the detachment condition using energy conservation principles. We finally validate our theoretical analysis by experimental data obtained in the explored ranges of the control parameters.

Key words: electrohydrodynamic effects, wetting and wicking, contact lines

1. Introduction

A sessile droplet on a flat dielectric-coated electrode wets the substrate more when a voltage is applied between the droplet and the electrode. The so-called electrowetting-on-dielectric (EWOD) phenomenon has been rapidly explored in recent years in both fundamental research and industrial applications. Spreading of droplets can be well controlled using the EWOD effect, making it an ideal tool to study contact-line dynamics including wetting, dewetting (Hong *et al.* 2014; Vo & Tran 2018), contact angle hysteresis (Nelson, Sen & Kim 2011; Sawane *et al.* 2015), droplet and soft-surfaces interactions (Dey *et al.* 2019), as well as coalescence-induced jumping droplets (Boreyko & Chen 2009; Farokhirad, Morris & Lee 2015; Vahabi *et al.* 2018). Moreover, EWOD has been emerging as a powerful technique in various industrial applications such as droplet manipulation (Fair *et al.* 2001; Fair 2007; Pollack, Fair & Shenderov 2000), optical

† Email addresses for correspondence: xuv1@pitt.edu, ttran@ntu.edu.sg

imaging systems (Berge & Peseux 2000; Kuiper & Hendriks 2004; Hao *et al.* 2014; Lee, Park & Chung 2019), liquid deposition (Baret & Brinkmann 2006; Leïchlé, Tanguy & Nicu 2007) and energy harvesting systems (Moon *et al.* 2013; Xu *et al.* 2020). An understanding of the droplet–substrate interactions under the electrowetting effect also helps in the design and optimisation of advanced surfaces such as anti-icing (Mishchenko *et al.* 2010) and self-cleaning surfaces (Blossey 2003).

Among applications utilising the electrowetting effect, induction of droplet detachment from a solid surface (Lee *et al.* 2014; Vo & Tran 2019; Wang *et al.* 2020; Weng *et al.* 2021; Xiao & Wu 2021) is not only a topic of fundamental interests, but also a versatile tool in enabling manipulation of droplets in three-dimensional settings (Hong *et al.* 2015; He *et al.* 2021). The principle of this technique relies on conversion of electrical energy to droplet surface energy by overstretching the droplet when the electrowetting effect is activated. Subsequently, when the electrowetting effect is deactivated, the excess surface energy of the overstretched droplet converts to kinetic energy inducing droplet retraction and detachment (Vo & Tran 2019). The critical condition of droplet detachment using electrowetting actuation is that the excess surface energy of the overstretched droplet overcomes the sum of viscous dissipation and elastic energy of the contact line during droplet retraction (Vo & Tran 2019).

In practice, in addition to the applied voltage used to control the strength of the electrowetting effect, the activating duration of the voltage T_p (see figure 1*a*, top panel) is also an important parameter determining jumping behaviours of the actuated droplets. Two major approaches to modulate T_p to induce droplet jumping by electrowetting are actuation from equilibrated state (AES) and actuation from maximum deformation state (AMS). In the AES approach (figure 1*a*, middle panel), the activating duration T_p is held until the droplet reaches its new equilibrium. In other words, T_p is set as $\geq \tau_e$, where τ_e is the time required for the droplet to reach the new equilibrium after the electrowetting effect is activated (Cavalli *et al.* 2016; Vo & Tran 2019; Wang *et al.* 2020). As τ_e is well defined using the system's parameters (Vo, Su & Tran 2018), the AES approach is simple and well controlled. However, the ability to induce droplet jumping using the AES method is limited by contact angle saturation, i.e. the electrowetting effect saturates at high applied voltage (Mugele & Baret 2005) resulting in a saturation of the excess surface energy supporting droplet detachment. In contrast, in the AMS approach (figure 1*a*, bottom panel), T_p is set equal to τ_m, i.e. the time for the droplet to reach maximum deformation state after the electrowetting effect is activated (Lee, Lee & Kang 2012; Lee *et al.* 2014). As the excess surface energy at the maximum deformation state is higher than that at the equilibrated state, the AMS method is a more effective approach compared to that using AES. For instance, for the same actuating system, the critical voltage for droplet detachment to occur from AMS is lower than that from AES (Lee *et al.* 2014; Wang *et al.* 2017). As a result, AMS is a more favourable method in practical applications (Hong & Lee 2015; Hong *et al.* 2015). Nevertheless, there is yet to be a parametric study on the dynamical behaviours of droplet detachment using AMS. Moreover, the critical conditions for droplet detachment using AMS is not yet established. This tremendously limits the applicability of the AMS method.

In this paper, we systematically investigate detachment behaviours of droplets under electrowetting actuation using the AMS method by varying three control parameters: applied voltage U, droplet viscosity μ and droplet radius r_0. We first confirm that the AMS method is a more effective approach to induce droplet detachment compared to that using AES shown by both a lower critical detachment voltage and higher maximum jumping

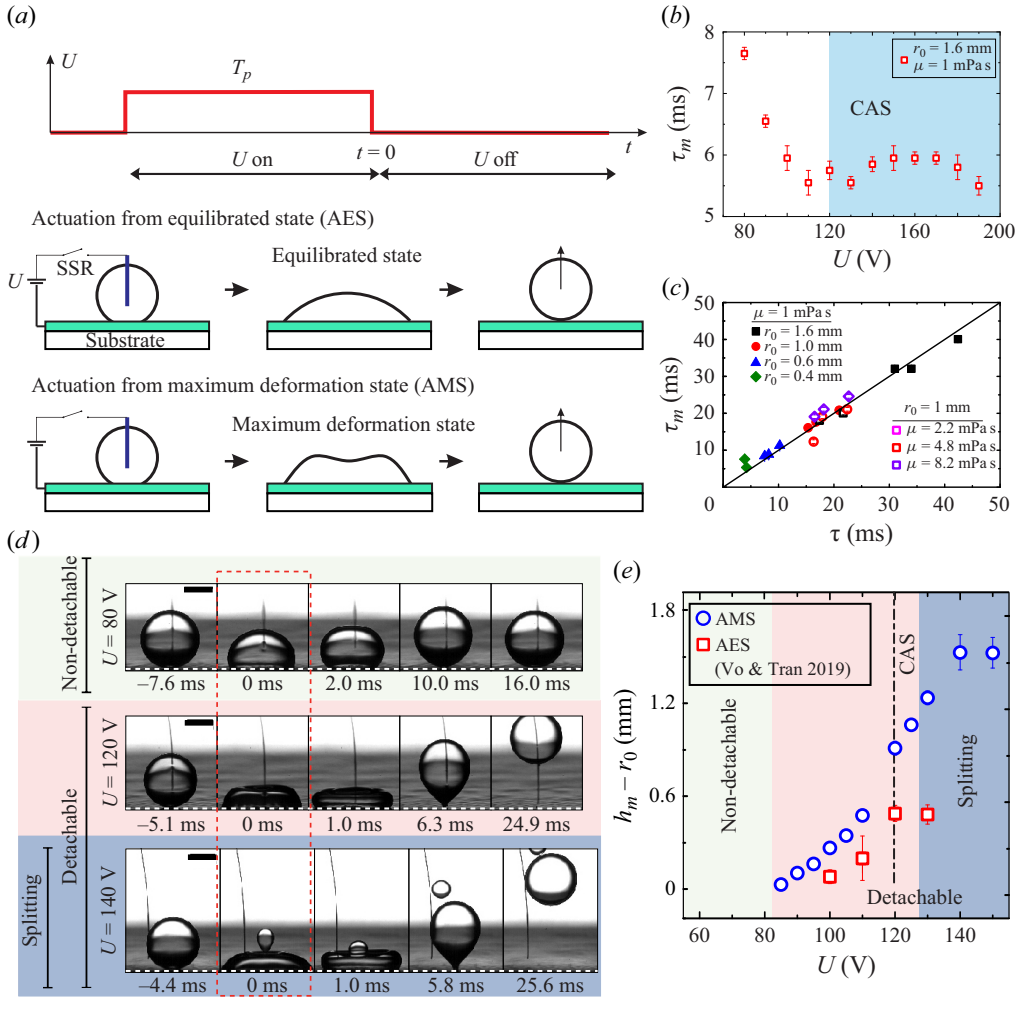

Figure 1. (*a*) Top panel, schematic illustrating modulation of the applied voltage. The duration of the voltage pulse is T_p and the time reference ($t = 0$) is set at the end of the pulse. Middle panel, schematic illustrating actuation from equilibrated state (AES). The voltage is turned on and maintained until the droplet reaches its equilibrated state; subsequently the voltage is turned off, causing droplet retraction. Bottom panel, schematic illustrating actuation from maximum deformation state (AMS). The voltage is turned on, causing a droplet to spread to its maximum deformation state, and is then turned off exactly at this moment. (*b*) Plot showing the time to reach maximum deformation, τ_m versus U. (*c*) Plot showing τ_m versus the underdamped characteristic spreading time $\tau = \pi(\rho r_0^3/\eta\sigma)^{1/2}$. The solid line represents the relation $\tau_m = \tau$. (*d*) Snapshots showing the behavioural change of a water droplet with radius 0.5 mm using AMS when U is increased. The scale bars represent 0.5 mm. (*e*) Plot showing the dependence of $h_m - r_0$ on U for droplets jumping from AMS (blue circles) and AES (red squares). Here, the droplet has radius $r_0 = 0.5$ mm and viscosity $\mu = 1.0$ mPa s; $U_s = 120$ V; the experiment was done in 2 cSt silicone oil.

height. We then construct a comprehensive phase diagram separating detachable and non-detachable behaviours of droplets under AMS varying all the three control parameters. The dependence of the detach velocity and detach time on the control parameters are also examined in detail. Finally, we theoretically develop and experimentally verify a model describing the critical condition for droplet detachment using the AMS approach.

%wt glycerol	μ (mPa s)	ρ (kg m^{-3})	σ (mN m^{-1})	U_s (V)
0	1.0	1000	37.2 ± 0.5	$\approx$120
20	2.2	1053	32.4 ± 1.0	$\approx$115
41.5	4.8	1106	30.4 ± 0.9	$\approx$110
55	8.2	1141	29.7 ± 0.5	$\approx$110
67	17.6	1174	26.9 ± 0.4	$\approx$105
74	32.7	1192	25.9 ± 0.5	$\approx$100
80	68.7	1210	26.8 ± 0.4	$\approx$105

Table 1. Measured values of viscosity μ, density ρ of glycerin solutions, and interfacial tensions σ between glycerin solutions and 2 cSt silicone oil. The CAS voltage U_s is determined experimentally by examining the saturation of the equilibrated contact angle θ_e when varying U (Vo & Tran 2019).

2. Experimental method

2.1. *Experimental set-up and materials*

To induce the electrowetting effect, we use a substrate made from an indium-tin-oxide (ITO) glass slide spin-coated with a layer of fluoropolymer (Teflon-1601, DuPont) (Vo & Tran 2021*a*). We set the thickness of the Teflon layer to $d = 2.5$ μm to ensure electrical insulation for the ITO electrode. To apply a voltage between a droplet deposited on the substrate and the ITO electrode, we use an 18 μm diameter tungsten wire dipped into the droplet bulk and connect it to the positive terminal of a direct current (DC) power supply via a normally open solid state relay (SSR) (see figure 1*a*). The negative terminal of the power supply is connected to the ITO electrode. We use a function generator to close the SSR, thereby applying a voltage U in the range $60\ \text{V} \leq U \leq 200\ \text{V}$ between the electrodes for a controlled duration T_p (figure 1*a*) to induce the electrowetting effect and droplet jumping. For our electrowetting substrates, the voltage causing contact angle saturation is $U_s \approx 110 \pm 10$ V (table 1).

We use aqueous glycerin solutions consisting of glycerol, DI water and 0.125 M sodium chloride to generate droplets. The electrical conductivity of the working liquid is measure experimentally at $\approx 8.8 \times 10^{-4}$ S m^{-1}. In our analysis and similar to other studies of electrowetting (Mugele & Baret 2005; Baret & Brinkmann 2006), we consider liquid droplets as perfectly conductive and neglect the minute effect of varying liquid permittivity. The viscosity μ of glycerin solutions is varied from 1.0 mPa s to 68.7 mPa s by adjusting the glycerol concentration (table 1). The droplet radius r_0 is also varied between 80μm and 1.5 mm. We immerse the substrate in a pool of silicone oil; the oil's temperature is kept at $20 \pm 0.5\,^{\circ}$C to maintain consistent experimental conditions. The use of silicone oil as the outer phase in our experiment is not only to reduce contact angle hysteresis, but also to increase initial contact angle of liquid droplets on the substrates (Baret & Brinkmann 2006; Hong & Lee 2015). The contact angle of glycerin solution droplets deposited on the substrate in the silicone oils is $\theta_0 = 160^{\circ}$ in the absence of the electrowetting effect. For simplicity, the viscosity of the oil is kept fixed at $\mu_o = 1.8$ mPa s. Other properties of the working liquids, including density ρ and interfacial tension σ, are measured experimentally and given in table 1.

To capture the behaviours of droplets under electrowetting actuation, we use a high-speed camera (Photron, SAX2), typically running at 5000 frames per second (FPS). The recorded images are processed using MATLAB to extract the contact radius r and dynamic contact angle θ_t during actuation, as well as the jumping height h of droplets after actuation. The measurements of r and θ_t, as well as the uncertainty analysis, follow

the same experimental procedure described in our previous study (Vo & Tran 2019). The uncertainty of the contact angle measurements is estimated within 2.5°. For each set of the control parameters (r_0, μ, U), the experiment is repeated three times.

2.2. *Electrowetting actuation*

To induce jumping of droplets using electrowetting actuation, we note that the activating duration T_p plays a crucial role. Experimental studies have pointed to the time to reach maximum deformation τ_m as the most optimal time duration for jumping droplets, i.e. causing highest jumping (Wang *et al.* 2017). We also note that the dynamics of droplets actuated by the electrowetting effect is either underdamped or overdamped, i.e. the electrowetting-induced driving force is opposed dominantly by either the droplet inertia or contact-line friction, respectively (Vo *et al.* 2018). Each one of these behaviours are characterised by a distinct spreading time scale. As it was shown that electrowetting-induced droplet detachment from solid substrates is only possible for spreading in the underdamped regime, we set the activating duration T_p equal to the underdamped characteristic spreading time $\tau = \pi(\rho r_0^3/\eta\sigma)^{1/2}$ (Vo *et al.* 2018; Wang *et al.* 2020; Xiao & Wu 2021):

$$T_p = \pi\left(\frac{\rho r_0^3}{\eta\sigma}\right)^{1/2}, \tag{2.1}$$

where the electrowetting number η, also known as the electrical capillary number (Fallah & Fattahi 2022; Hassan *et al.* 2023), is defined as $\eta = \epsilon\epsilon_0 U^2/(2d\sigma)$ for $U \le U_s$ and $\eta = \epsilon\epsilon_0 U_s^2/(2d\sigma)$ for $U > U_s$. Here, ϵ and d respectively are the dielectric constant and thickness of the Teflon coating, ϵ_0 the permittivity of free space, ρ the droplet density, σ the droplet–oil interfacial tension and $U_s \approx 110 \pm 10$ V the threshold voltage above which contact angle saturation (CAS) occurs. The threshold voltage U_s is determined experimentally by examining the dependence of the equilibrated contact angle θ_e on the applied voltage U (Vo & Tran 2021*b*). Slight fluctuation of U_s is within ± 10 V and occurs when varying the liquid's viscosity (see table 1). We note that (2.1) implies that T_p also saturates when $U > U_s$ due to the contact angle saturation effect, consistent with the experimental data shown in figure 1(*b*). In figure 1(*c*), we show an excellent agreement between the measured values of the time to reach maximum deformation and the characteristic spreading time τ of droplets actuation in the underdamped regime. This strongly suggests that τ can be used to describe the time to reach maximum deformation of droplets under electrowetting actuation. As a result, the activating duration T_p in our experiment is determined by (2.1), i.e. dependent only on the experimental parameters and free of uncertainty from the experimental values of τ_m.

3. Results and discussions

3.1. *Droplet jumping by EWOD actuation from maximum deformation state*

In figure 1(*d*), we show several series of snapshots of actuated droplets to illustrate their spreading and jumping dynamics. From the top panel to the bottom one, the applied voltage U is increased from 80 V to 140 V, while the droplet radius and viscosity are fixed at $r_0 = 0.5$ mm and $\mu = 1.0$ mPa s, respectively. Generally, we observe that as soon as the electrowetting effect is activated on a droplet, it causes droplet spreading with an initial contact-line velocity v_I and generates on the droplet's surface capillary waves propagating from the contact line towards the apex. At the end of the activating duration ($t = 0$), the

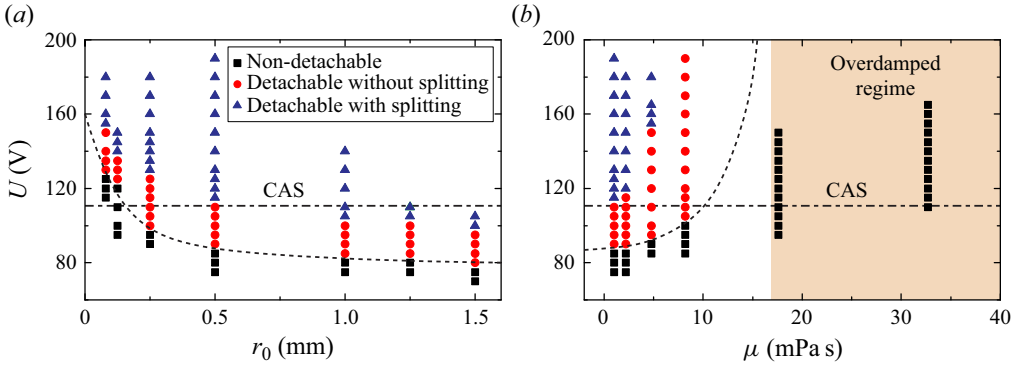

Figure 2. (*a*) Phase diagram showing different behaviours of $\mu = 1.0$ mPa s droplets under AMS with varying U and r_0. (*b*) Phase diagram showing different behaviours of $r_0 = 0.5$ mm droplets under AMS with varying U and μ. In both diagrams, droplet behaviours are categorised into three major regimes: non-detachable (black squares), detachable without splitting (red circles) and detachable with splitting (blue triangles). The dash lines are used to guide the eyes along the boundary between the detachable and the non-detachable regimes. The dash-dotted lines indicate the average contact angle saturation (CAS) threshold (see table 1 for specific values of U_s at different μ).

droplet immediately recoils and subsequently jumps off from the substrate if the applied voltage is sufficiently high. For instance, in the experiment shown in figure 1(*d*), droplet detachment from the solid substrate occurs for $U \geq 90$ V. We also observe that at high applied voltages, e.g. $U = 140$ V (figure 1*d*, last panel), a small satellite droplet is ejected from the actuated droplet. This is due to the effect of the strong capillary waves on the droplet's surface generated by the electrowetting effect (Vo & Tran 2021*b*).

In the cases where an actuated droplet detaches from the substrate, the detach time T_d, measured from the time reference $t = 0$ to the moment the droplet detaches, reduces with the applied voltage. For instance, T_d drops from 6.3 ms to 5.8 ms when U increases from 120 V to 140 V (figure 1*d*). Moreover, the maximum jumping height h_m defined as the maximum height of the droplet's centre of mass increases with U. For instance, $h_m - r_0$ significantly increases from 0.38 mm to 1.55 mm when U increases from 100 V to 140 V (figure 1*d*). Comparing the maximum jumping height obtained in our experiment with that obtained in the case where jumping is induced by AES (figure 1*e*), we observe that for the same voltage, h_m obtained from AMS (blue circles) is consistently higher than that from AES (red squares). Moreover, the maximum jumping height obtained from AMS is not limited by contact angle saturation, in contrast to that from AES.

In figure 2, we show the phase diagrams of droplet behaviours obtained by varying three of the control parameters r_0, μ and U. These observed behaviours, which are illustrated in figure 1(*d*), include non-detachable, detachable without splitting and detachable with splitting. The critical voltage at the transition for detachment is higher for smaller droplet size (figure 2*a*) or higher viscosity (figure 2*b*). We also observe that the detachment of droplet is limited for $\mu < 17.6$ mPa s as the transition from the underdamped regime to overdamped regime occurs at 17.6 mPa s (figure 2*b*) (Vo *et al.* 2018). We highlight that the AMS method works for r_0 as small as 80 μm, a limit that was not possible using AES for the same substrate (Vo & Tran 2019).

3.2. *Detach velocity and detach time*

In the case where a droplet detaches from the solid substrate, the detach velocity u_d, defined as the droplet's centre-of-mass velocity at the moment it completely separates from

the substrate, and the detach time T_d, i.e. the duration from the reference time $t = 0$ to the separating moment, are the most critical parameters representing the detaching dynamics. Understanding of these characteristic parameters help optimise design and operations of droplet-actuating systems using the electrowetting effect. In this section, we discuss the dependencies of u_d and T_d on the applied voltage U, viscosity μ and droplet radius r_0.

We first focus on the detach velocity u_d. In figure 3(a), we show the dependence of u_d on the applied voltage U for r_0 varying from 0.08 mm to 1.25 mm and μ fixed at 1 mPa s. Generally, we observe that u_d increases with U as a result of higher electrical energy applied to the system. However, the dependence of u_d on U becomes more irregular at high applied voltage, i.e. $U > 130$ V. For example, for $r_0 = 0.08$ mm, u_d varies little between $U = 140$ V and $U = 150$ V. We attribute such irregular dependence of u_d on U to hydrodynamical and electrical instabilities of the system at high voltage. When the applied voltage increases, the electrical force applied to the contact line becomes larger, causing more abrupt and forceful deformation to the droplet, e.g. stronger capillary waves and even splitting of the droplet (figure 1d). Such violent behaviours induce nonlinear effects that reduce the energy transfer efficiency, from electrical to kinetic energy of the detached droplet. Moreover, electrical leakage may be possible through the dielectric layer at high applied voltage without breaking it down during the experiment (Moon *et al.* 2002). This also reduces the efficiency of the EWOD effect in generating higher u_d for jumping droplets. Therefore, reducing irregularities at high voltage may require increasing viscosities of the liquids or using insulators with higher dielectric strength. Next, in figure 3(b), we plot the dependence of u_d on U for μ varying from 1 mPa s to 8.2 mPa s and r_0 fixed at 0.5 mm. We observe that for $U < 130$ V, u_d linearly increases with U, whereas for $U \geq 130$ V, u_d approaches a plateau. The increasing rate of u_d with U also reduces with higher μ due to larger viscous dissipation.

We now examine the detach time T_d. In figures 3(c) and 3(d), we respectively show T_d versus U for various droplet radii and droplet viscosities. We note that for $r_0 = 1.25$ mm and $r_0 = 1.5$ mm, the voltage is limited at 110 V and 100 V, respectively, due to frequent electrical breakdowns of the dielectric layer separating the electrode and the liquids. Here, electrical breakdowns increase with the actuation time, as well as the contact area between the droplet and the substrate during actuation. Both factors increase with larger droplet radius.

Typically, T_d decreases with increasing U as long as the voltage is within the contact angle saturation (CAS) limit, i.e. $U_s = 110$ V in our case. The detach time T_d eventually reaches a plateau when the applied voltage exceeds U_s. Here, we note that T_d for AMS is defined in the same way as the droplet's retracting time, i.e. from the moment the electrowetting effect is turned off at the droplet's maximum deformation to the moment the droplet detaches from the surface. In addition, the retracting time of the droplet only depends on its maximum spreading diameter, which is limited by CAS. As a result, we infer that T_d also saturates when $U \geq U_s$, consistent with our experimental results shown in figures 3(c) and 3(d).

The detach time T_d, which is measured from the moment the voltage is released to the detaching moment, is defined in the same way as the retracting time of the droplets from maximum deformation. As a result, we hypothesise that T_d is closely related to the time scale characterising the spreading (or retracting) dynamics of droplets. As the spreading droplets in our study are underdamped, we examine the relation between T_d and the underdamped characteristic spreading time scale τ and show a plot of T_d versus τ in figure 3(e). The plot consists of data obtained by varying r_0, μ and U in their explored ranges. We observe that the dependence of T_d on τ can be approximately described

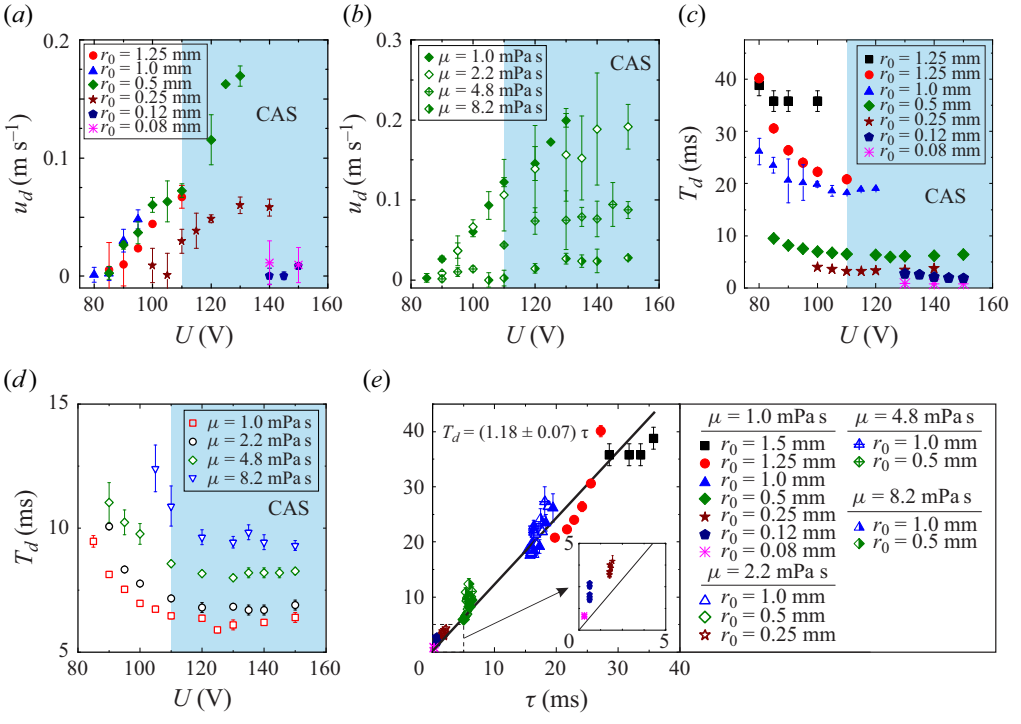

Figure 3. (*a*,*b*) Plots showing detach velocity u_d versus U for (*a*) different droplet radii r_0 and (*b*) different droplet viscosity μ. (*c*,*d*) Plots showing detach time T_d versus U for (*c*) different droplet radii r_0 and (*d*) different droplet viscosity μ. (*e*) Plot showing detach time T_d versus τ for various values of r_0, U and μ. Inset is a zoomed-in plot showing data in the dashed box. The solid line indicates the best fit to the experimental data using the linear relation $T_d = k\tau$, where $k = 1.18 \pm 0.07$. The shaded areas indicate the average contact angle saturation (CAS) threshold (see table 1 for specific values of U_s for different μ).

using a linear relation $T_d \approx k\tau$, where $k = 1.18 \pm 0.07$, suggesting that T_d is reasonably characterised by τ in the explored ranges of the control parameters. Furthermore, for each dataset obtained using fixed μ and r_0, we note that figures 3(*c*) and 3(*d*) indicate that T_d decreases with U for $U < U_s$ and plateaus for $U > U_s$. This implies smaller data deviation from the linear fit in figure 3(*e*) at higher voltages. In other words, the linear fit better describes the relation between T_d and τ in the high-voltage regime.

3.3. *Critical conditions for jumping droplets by EWOD actuation from maximum deformation state*

We now search for the critical condition for droplet detachment by AMS. We first note that the droplet actuation dynamics in our study is kept in the underdamped regime, as it is the requirement to enable detachment (Vo & Tran 2019). This requirement also ensures that the excess surface energy at the maximum deformation state is not entirely dissipated by the viscous effect during retraction. Subsequently, we follow the energy balance approach used to determine the jumping conditions for droplets actuated by AES (Vo & Tran 2019) to formulate the critical condition for droplets to detach from the solid substrate by AMS as

$$\Delta E_s \geq E_v + E_{cl}, \tag{3.1}$$

where $\Delta E_s = E_s^m - E_s^d$ is the difference between the surface energy at maximum deformation E_s^m and the surface energy at the detach moment E_s^d; E_v is the viscous dissipation and E_{cl} contact line elasticity energy during retraction. We note that the kinetic energy of a droplet vanishes at its maximum deformation state. The gravitational potential energy is negligible compared with the surface energy as the Bond number $Bo = (\rho - \rho_o) g r_0^2 \sigma^{-1}$ is small ($2.14 \times 10^{-4} \leq Bo \leq 1.23 \times 10^{-1}$). Here, $\rho_o = 873$ kg m^{-3} is the density of silicone oil and $g = 9.81$ m s^{-2} is the gravitational acceleration.

We first focus on the surface energy difference ΔE_s and note that it can be written as $\Delta E_s = E_s^m - E_s^e + E_s^e - E_s^d$, where E_s^e is the surface energy at equilibrated state after applying the electrowetting effect without turning it off. On one hand, we note that the surface energy difference $E_s^e - E_s^d$ between the equilibrated state and detachment was already formulated (Vo & Tran 2019): $E_s^e - E_s^d = [2(1 + \cos\theta_e)^{-1} - 4(r_0/r_e)^2 - \cos\theta_0]\sigma\pi r_e^2$, where θ_e, r_e are respectively the contact angle and contact radius of the droplet at the equilibrated state; θ_0 is the contact angle of the droplet at the initial state. Moreover, we argue that the surface energy difference $E_s^m - E_s^e$ comes from the capillary wave generated at the beginning of droplet actuation; this wave would not occur if the voltage U were to ramp up slowly to keep the spreading quasi-static. As a result, the surface energy difference $E_s^m - E_s^e$ is calculated by the energy carried by the capillary wave $E_s^m - E_s^e = 0.5\rho a^2 \omega^2 lS$, where $a \sim r_0 We^{1/2} \sin\theta_0 (T_p\omega)^{2/3}/[2\pi(1-\xi^2)^{1/2}]$ is the wave amplitude at time $t = T_p$; $\omega \sim (\sigma/\rho r_0^3)^{1/2}$ is the angular frequency of the wave; $l \sim r_0$ is the wavelength; $\xi = \lambda/(\sigma\rho r_0)^{1/2}$ is the decaying ratio of the capillary waves; λ is the contact line friction coefficient; $S = 2(1 + \cos\theta_e)^{-1}\pi r_e^2$ is the area of a hypothetical spherical cap having contact angle θ_e and base radius r_e; and We is the contact line Weber number, defined to directly relate to the applied voltage U by the relation $We = [(\epsilon\epsilon_0/2d\sigma)^{1/2}(U - U_c) + 1]^2$. Here, U_c is the critical voltage for capillary wave generation on the droplet's surface (Vo & Tran 2021*b*). In our experiment, U_c varies from 70 V to 110 V depending on the viscosity and radius of the actuated droplet. We therefore obtain the expression of the surface energy difference:

$$\Delta E_s = \left[\frac{2}{1+\cos\theta_e} - 4\left(\frac{r_0}{r_e}\right)^2 - \cos\theta_0 + We\frac{(T_p\omega)^{4/3}}{4\pi^2(1-\xi^2)}\frac{\sin^2\theta_0}{1+\cos\theta_e}\right]\sigma\pi r_e^2. \quad (3.2)$$

We note that the damping ratio ξ is essentially similar to the Ohnesorge number $\mathrm{Oh} = \mu(\sigma\rho r_0)^{-1/2}$ in which the contact line friction coefficient λ is used instead of the liquid's viscosity μ to represent dissipation. In our analysis, λ is obtained empirically using the relation $\lambda = C(\mu\mu_o)^{1/2}$, where $C = 32.9$ is a fitting parameter (Vo *et al.* 2018; Vo & Tran 2019). By using ξ instead of Oh, the dissipation in the liquid bulk is effectively neglected (Carlson, Bellani & Amberg 2012*a*,*b*; Vo & Tran 2019). Indeed, the ratio ξ/Oh, calculated for all of our experiments, varies from 5.47 to 45.3, strongly suggesting that the dissipation at the contact line is dominant. As a result, we ignore bulk dissipation in our estimation of $E_s^m - E_s^e$ to arrive at (3.2). Also, by only considering dissipation at the contact line, we obtain an expression for E_v (Vo & Tran 2019):

$$E_v \sim \lambda\frac{r_m}{T_d}\pi r_m^2 \approx \lambda\frac{r_e}{T_d}\pi r_e^2. \quad (3.3)$$

The contact line elasticity energy E_{cl} is the surface energy accumulation due to pinning and subsequent stretching of the liquid–oil interface at the vicinity of the contact line (Joanny & de Gennes 1984; Vo & Tran 2019) and is determined by a similar approach to

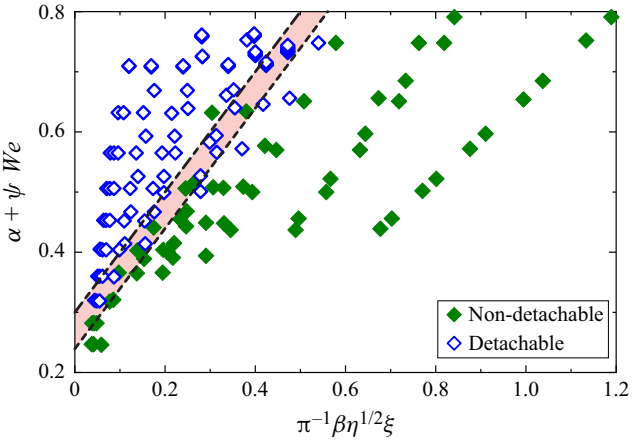

Figure 4. Plot showing $\alpha + \Psi\ We$ versus $\pi^{-1}\beta\eta^{1/2}\xi$ using the data of the non-detachable and detachable behaviours shown in figure 2. The shaded area indicates the transitional extent due to variation in κ ($\kappa = 0.27 \pm 0.03$).

that of Vo & Tran (2019):

$$E_{cl} \sim \kappa\sigma\,\pi r_m^2 \approx \kappa\sigma\,\pi r_e^2. \tag{3.4}$$

Here, $\kappa = \pi \sin^2\theta_r / \ln(r_0/\gamma)$, where θ_r is the receding contact angle and γ is the defect's size. In our experiment, which was conducted using the same set-up and materials as Vo & Tran (2019), $\theta_r \approx 121^\circ$ and the average defect's size is $\gamma \approx 260$ nm. The parameter κ only changes minutely within the explored droplet radius: $\kappa = 0.27 \pm 0.03$ for $0.08\ \text{mm} \leq r_0 \leq 1.25$ mm.

Substituting (3.2), (3.3), (3.4) into (3.1), the condition at the transition between non-detachable and detachable behaviours is

$$\frac{2}{1+\cos\theta_e} - 4\left(\frac{r_0}{r_e}\right)^2 - \cos\theta_0 + We\frac{(T_p\omega)^{4/3}}{4\pi^2(1-\xi^2)}\frac{\sin^2\theta_0}{1+\cos\theta_e} = \frac{r_e\lambda}{T_d\sigma} + \kappa. \tag{3.5}$$

As shown in the previous sections, both the activation time T_p and the detach time T_d are well approximated by the underdamped characteristic spreading time τ. We therefore simplify (3.5) as

$$\alpha + \Psi(\theta_e, \xi)We = \pi^{-1}\beta\eta^{1/2}\xi + \kappa, \tag{3.6}$$

where $\beta = r_e/r_0 = (1-\cos\theta_e^2)^{1/2}[4(1-\cos\theta_e)^{-2}(2+\cos\theta_e)^{-1}]^{1/3}$, $\alpha = 2(1+\cos\theta_e)^{-1} - 4\beta^{-2} - \cos\theta_0$, and $\Psi(\theta_e, \xi) = 0.25\sin^2\theta_0(1+\cos\theta_e)^{-1}(\pi\eta)^{-2/3}(1-\xi^2)^{-1}$. We note that θ_e depends on the electrowetting number η following the Young–Lippmann equation $\cos\theta_e - \cos\theta_0 = \eta$ (Mugele & Baret 2005).

In figure 4, we show a plot of $\alpha + \Psi\ We$ versus $\pi^{-1}\beta\eta^{1/2}\xi$ of all the data obtained for the non-detachable and detachable behaviours shown in figure 2. Here, the composite terms $\alpha + \Psi\ We$ and $\pi^{-1}\beta\eta^{1/2}\xi$ respectively represent the driving energy and the energy cost for detachment. The shaded area indicates the transitional extent caused by variation in κ ($\kappa = 0.27 \pm 0.03$) resulting from variations in both the defect's size γ and the radius r_0. We note that all the terms in (3.6) are calculated using the system parameters except the contact line friction coefficient, which is determined empirically using $\lambda = C(\mu\mu_o)^{1/2}$ with $C = 32.9$ (Vo *et al.* 2018; Vo & Tran 2019), and the receding contact angle $\theta_r \approx 121^\circ$

determined independently from our previous work (Vo & Tran 2019). The excellent agreement between the experimental data and the formulated jumping condition (3.6) thus highlights our analysis as a predictive tool for utilizing modulated electrowetting in droplet actuation and detachment from surfaces.

4. Conclusions

We aim to systematically investigate droplet detachment induced by EWOD using actuation from the maximum deformation state (AMS). By varying droplet radius, viscosity and applied voltage, we demonstrate a significant expansion of the detachable regime for droplets actuated by using the electrowetting effect with AMS and provide a comprehensive phase diagram of the detachment behaviours. The applied voltage for AMS, no longer bounded by contact angle saturation limit, enables detachment of droplets as small as 80 μm in radius. This introduces a powerful tool for applications requiring actuation and detachment of droplets from solid surfaces, in particular, those dealing with small droplets or highly viscous liquids. We then provide a detailed characterisation of detach velocity and detach time of actuated droplets. Finally, we develop a theoretical prediction for the critical condition causing droplet detachment. The theoretical prediction is consistent with our experimental data for liquid viscosity ranging from 1 mPa to 68.7 mPa, droplet size from 0.08 mm to 1.5 mm and applied voltage from 60 V to 200 V.

We note that our study is limited within the droplet-in-oil setting and further studies may be required to explore the limit of our analysis in the droplet-in-air setting, which is typically known for stronger hysteresis effect and electrical instability at the three-phase contact line. Nevertheless, our study may serve as a strong basis for wider use of electrowetting in applications requiring precise actuation of droplets such as tissue engineering, digital microfluidics and three-dimensional (3-D) printing. Our results also provide key insights to mechanistic understanding of related phenomena such as coalescence-induced jumping of droplets (Boreyko & Chen 2009; Liu *et al.* 2014; Farokhirad *et al.* 2015) or droplet bouncing on solid substrates (Sanjay, Chantelot & Lohse 2023).

Funding. This study is supported by Nanyang Technological University, the Republic of Singapore's Ministry of Education (MOE, grant number MOE2018-T2-2-113), and the RIE2020 Industry Alignment Fund–Industry Collaboration Projects (IAF–ICP) Funding Initiative, as well as cash and in-kind contribution from the industry partner, HP Inc.

Declaration of interests. The authors report no conflict of interest.

Author ORCIDs.
Quoc Vo https://orcid.org/0000-0002-2270-1532;
Tuan Tran https://orcid.org/0000-0002-5132-6495.

References

Baret, J.-C. & Brinkmann, M. 2006 Wettability control of droplet deposition and detachment. *Phys. Rev. Lett.* **96** (14), 146106.

Berge, B. & Peseux, J. 2000 Variable focal lens controlled by an external voltage: an application of electrowetting. *Eur. Phys. J.* E **3** (3), 159–163.

Blossey, R. 2003 Self-cleaning surfaces — virtual realities. *Nat. Mater.* **2** (5), 301–306.

Boreyko, J.B. & Chen, C.H. 2009 Self-propelled dropwise condensate on superhydrophobic surfaces. *Phys. Rev. Lett.* **103** (18), 2–5.

Carlson, A., Bellani, G. & Amberg, G. 2012*a* Contact line dissipation in short-time dynamic wetting. *Europhys. Lett.* **97** (4), 44004.

CARLSON, A., BELLANI, G. & AMBERG, G. 2012*b* Universality in dynamic wetting dominated by contact-line friction. *Phys. Rev.* E **85** (4), 045302.

CAVALLI, A., PRESTON, D.J., TIO, E., MARTIN, D.W., MILJKOVIC, N., WANG, E.N., BLANCHETTE, F. & BUSH, J.W.M. 2016 Electrically induced drop detachment and ejection. *Phys. Fluids* **28** (2), 022101.

DEY, R., VAN GORCUM, M., MUGELE, F. & SNOEIJER, J.H. 2019 Soft electrowetting. *Soft Matt.* **15** (32), 6469–6475.

FAIR, R.B., POLLACK, M.G., WOO, R., PAMULA, V.K., HONG, R., ZHANG, T. & VENKATRAMAN, J. 2001 A micro-watt metal-insulator-solution-transport (MIST) device for scalable digital bio-microfluidic systems. In *IEEE International Electron Devices Meeting. Technical Digest* (cat. no. 01CH37224), pp. 16.4.1–16.4.4.

FAIR, R.B. 2007 Digital microfluidics: is a true lab-on-a-chip possible? *Microfluid Nanofluid* **3** (3), 245–281.

FALLAH, K. & FATTAHI, E. 2022 Splitting of droplet with different sizes inside a symmetric T-junction microchannel using an electric field. *Sci. Rep.* **12** (1), 1–12.

FAROKHIRAD, S., MORRIS, J.F. & LEE, T. 2015 Coalescence-induced jumping of droplet: inertia and viscosity effects. *Phys. Fluids* **27** (10), 102102.

HAO, C., LIU, Y., CHEN, X., HE, Y., LI, Q., LI, K.Y. & WANG, Z. 2014 Electrowetting on liquid-infused film (EWOLF): complete reversibility and controlled droplet oscillation suppression for fast optical imaging. *Sci. Rep.* **4** (1), 6846.

HASSAN, R.UL., KHALIL, S.M., KHAN, S.A., MOON, J., CHO, D.H. & BYUN, D. 2023 Electric field and viscous fluid polarity effects on capillary-driven flow dynamics between parallel plates. *Heliyon* **9** (6), e16395.

HE, X., ZHANG, J., YANG, B., ZHANG, X. & DENG, Y. 2021 Droplet three-dimension manipulation in parallel liquid-infused membrane plates configuration. *Sensor. Actuat.* A*: Phys.* **330**, 129344.

HONG, J., KIM, Y.K., KANG, K.H., KIM, J. & LEE, S.J. 2014 Spreading dynamics and oil film entrapment of sessile drops submerged in oil driven by DC electrowetting. *Sensor. Actuat.* B*: Chem.* **196**, 292–297.

HONG, J., KIM, Y.K., WON, D.-J., KIM, J. & LEE, S.J. 2015 Three-dimensional digital microfluidic manipulation of droplets in oil medium. *Sci. Rep.* **5** (1), 10685.

HONG, J. & LEE, S.J. 2015 Detaching droplets in immiscible fluids from a solid substrate with the help of electrowetting. *Lab on a chip* **15** (3), 900–907.

JOANNY, J.F. & DE GENNES, P.G. 1984 A model for contact angle hysteresis. *J. Chem. Phys.* **81** (1), 552–562.

LEE, S.J., LEE, S. & KANG, K.H. 2012 Droplet jumping by electrowetting and its application to the three-dimensional digital microfluidics. *Appl. Phys. Lett.* **100** (8), 081604.

KUIPER, S. & HENDRIKS, B.H.W. 2004 Variable-focus liquid lens for miniature cameras. *Appl. Phys. Lett.* **85** (7), 1128–1130.

LEE, J., PARK, Y. & CHUNG, S.K. 2019 Multifunctional liquid lens for variable focus and aperture. *Sensor. Actuat.* A*: Phys.* **287**, 177–184.

LEE, S.J., HONG, J., KANG, K.H., KANG, I.S. & LEE, S.J. 2014 Electrowetting-induced droplet detachment from hydrophobic surfaces. *Langmuir* **30** (7), 1805–1811.

LEÏCHLÉ, T., TANGUY, L. & NICU, L. 2007 Electrowetting-assisted drop deposition for controlled spotting. *Appl. Phys. Lett.* **91** (22), 224102.

LIU, F., GHIGLIOTTI, G., FENG, J.J. & CHEN, C.H. 2014 Numerical simulations of self-propelled jumping upon drop coalescence on non-wetting surfaces. *J. Fluid Mech.* **752**, 39–65.

MISHCHENKO, L., HATTON, B., BAHADUR, V., TAYLOR, J.A., KRUPENKIN, T. & AIZENBERG, J. 2010 Design of ice-free nanostructured surfaces based on repulsion of impacting water droplets. *ACS Nano* **4** (12), 7699–7707.

MOON, H., CHO, S.K., GARRELL, R.L. & KIM, C.-J. 2002 Low voltage electrowetting-on-dielectric. *J. Appl. Phys.* **92** (7), 4080–4087.

MOON, J.K., JEONG, J., LEE, D. & PAK, H.K. 2013 Electrical power generation by mechanically modulating electrical double layers. *Nat. Commun.* **4** (1), 1486–1487.

MUGELE, F. & BARET, J.-C. 2005 Electrowetting: from basics to applications. *J. Phys.: Condens. Matter* **17** (28), R705–R774.

NELSON, W.C., SEN, P. & KIM, C.-J. 2011 Dynamic contact angles and hysteresis under electrowetting-on-dielectric. *Langmuir* **27** (16), 10319–10326.

POLLACK, M.G., FAIR, R.B. & SHENDEROV, A.D. 2000 Electrowetting-based actuation of liquid droplets for microfluidic applications. *Appl. Phys. Lett.* **77** (11), 1725–1726.

SANJAY, V., CHANTELOT, P. & LOHSE, D. 2023 When does an impacting drop stop bouncing? *J. Fluid Mech.* **958**, 1–20.

SAWANE, Y.B., DATAR, S., OGALE, S.B. & BANPURKAR, A.G. 2015 Hysteretic DC electrowetting by field-induced nano-structurations on polystyrene films. *Soft Matt.* **11** (13), 2655–2664.

VAHABI, H., WANG, W., MABRY, J.M. & KOTA, A.K. 2018 Coalescence-induced jumping of droplets on superomniphobic surfaces with macrotexture. *Sci. Adv.* **4** (11), 1–8.

VO, Q., SU, H. & TRAN, T. 2018 Universal transient dynamics of electrowetting droplets. *Sci. Rep.* **8** (1), 836.

VO, Q. & TRAN, T. 2018 Contact line friction of electrowetting actuated viscous droplets. *Phys. Rev.* E **97** (6), 063101.

VO, Q. & TRAN, T. 2019 Critical conditions for jumping droplets. *Phys. Rev. Lett.* **123** (2), 24502.

VO, Q. & TRAN, T. 2021*a* Droplet ejection by electrowetting actuation. *Appl. Phys. Lett.* **118** (16), 161603.

VO, Q. & TRAN, T. 2021*b* Dynamics of droplets under electrowetting effect with voltages exceeding the contact angle saturation threshold. *J. Fluid Mech.* **925**, A19.

WANG, Q., XU, M., WANG, C., GU, J., HU, N., LYU, J. & YAO, W. 2020 Actuation of a nonconductive droplet in an aqueous fluid by reversed electrowetting effect. *Langmuir* **36** (28), 8152–8164.

WANG, Z., VAN DEN ENDE, D., PIT, A., LAGRAAUW, R., WIJNPERLÉ, D. & MUGELE, F. 2017 Jumping drops on hydrophobic surfaces, controlling energy transfer by timed electric actuation. *Soft Matt.* **13** (28), 4856–4863.

WENG, N., WANG, Q., GU, J., LI, J., WANG, C. & YAO, W. 2021 The dynamics of droplet detachment in reversed electrowetting (REW). *Colloids Surf. (*A*)* **616** (104), 126303.

XIAO, K. & WU, C.X. 2021 Curvature effect of electrowetting-induced droplet detachment. *J. Appl. Phys.* **129** (23), 234701.

XU, W., *et al.*2020 A droplet-based electricity generator with high instantaneous power density. *Nature* **578** (7795), 392–396.